Effect of Cu^{2+} substitution in spin-orbit coupled $Sr_2Ir_{1-x}Cu_xO_4$: Structure, magnetism, and electronic properties

Imtiaz Noor Bhatti,[1] R. S. Dhaka,[2] and A. K. Pramanik[1,*]

[1]*School of Physical Sciences, Jawaharlal Nehru University, New Delhi 110067, India*

[2]*Department of Physics, Indian Institute of Technology Delhi, Hauz Khas, New Delhi 110016, India*

(Received 6 September 2017; revised manuscript received 10 October 2017; published 26 October 2017)

Sr_2IrO_4 is an extensively studied spin-orbit coupling induced insulator with antiferromagnetic ground state. The delicate balance between competing energy scales plays a crucial role for its low-temperature phase and the route of chemical substitution has often been used to tune these different energy scales. Here, we report an evolution of structural, magnetic, and electronic properties in doped $Sr_2Ir_{1-x}Cu_xO_4$ ($x \leqslant 0.2$). The substitution of Cu^{2+} ($3d^9$) for Ir^{4+} ($5d^5$) acts for electron doping, though it tunes the related parameters such as spin-orbit coupling, electron correlation, and Ir charge state. Moreover, both Ir^{4+} and Cu^{2+} has single unpaired spin, though it occupies different d orbitals. With Cu substitution, the system retains its original structural symmetry but the structural parameters show systematic changes. X-ray photoemission spectroscopy measurements show that Ir^{4+} equivalently converts to Ir^{5+} and a significant enhancement in the density of states has been observed at the Fermi level due to the contribution from the Cu $3d$ orbitals, which supports the observed decrease in the resistivity with Cu substitution. While the long-range magnetic ordering is much weakened and the highest-doped sample shows almost paramagneticlike behavior, the overall system remains insulator. Analysis of the resistivity data shows a mode of charge conduction in the whole series follows a two-dimensional variable-range-hopping model, but the range of validity varies with temperature. The whole series of samples exhibits negative magnetoresistance at low temperature, which is considered to be a signature of a weak-localization effect in a spin-orbit coupled system, and its evolution with Cu appears to follow the variation of resistivity with x.

DOI: 10.1103/PhysRevB.96.144433

I. INTRODUCTION

In recent times, Ir-based oxides have been the most extensively studied materials for their many interesting properties [1–10]. The layered Sr_2IrO_4 is of prime interest due to its exotic $J_{\text{eff}} = 1/2$ ground state. The Ir in Sr_2IrO_4 adopts an ionic state of Ir^{4+} which has $5d^5$ electronic configuration. The crystal-field effect (CFE) in the IrO_6 octahedral environment splits the $5d$ orbital into t_{2g} and e_g levels; then, in the presence of a strong spin-orbit coupling (SOC) effect, the low-lying t_{2g} level is further split into a fully filled $J_{\text{eff}} = 3/2$ quartet and a partially filled $J_{\text{eff}} = 1/2$ doublet state [10,11]. These $J_{\text{eff}} = 1/2$ pseudospins engage in a Heisenberg-type antiferromagnetic (AFM) exchange interaction; however, the rotation or distortion of IrO_6 octahedra induces a Dzyaloshinskii-Moriya (DM)-type antisymmetric interaction, which is believed to give rise to weak ferromagnetic (FM) behavior in this material [12,13].

The bilayer nature of Sr_2IrO_4 is very evident in an asymmetric magnetic exchange interaction along the in-plane and out-of-plane directions [14]. Moreover, experimental studies have shown that the evolution of magnetism is strongly linked to its structural modifications [15,16]. This material is surprisingly an insulator with extended $5d$ orbitals which provides a low electronic correlation effect (U), and hence Sr_2IrO_4 would otherwise be a metal. In addition, following structural symmetry with other $3d$- and $4d$-based superconducting (SC) materials, i.e., doped La_2CuO_4 [17,18] and Sr_2RuO_4 [19,20], respectively, the recent theoretical studies have predicted a possible SC state in doped Sr_2IrO_4 [21–25]. While experimental data have not supported any SC state to date, the angle-resolved photoemission spectroscopy (ARPES) measurements have interestingly shown some exotic electronic states in doped Sr_2IrO_4, such as disconnected Fermi arcs and rapid collapse of Mott gap with the emergence of nodal excitations, where these features are similarly seen in doped cuprates [26,27].

With an aim to understand the exotic magnetic ground state as well as to tune the electronic properties for the realization of possible SC behavior, the approach of chemical substitution with various elements has recently been adopted both at the Sr and Ir sites. For instance, the collapse of the long-range magnetic state and the evolution of metallic behavior have generally been observed in the case of electron doping of $(Sr_{1-x}La_x)IrO_4$ [28,29]. Some of the Ir-site doping has yielded similar results. The Rh substitution in $Sr_2Ir_{1-x}Rh_xO_4$ has shown suppression of both the ordered magnetic and insulating state where the system evolves to a paramagnetic (PM) and metallic state above a critical concentration of Rh in the system [30,31]. Similarly, Ru substitution has caused suppression of magnetic ordering in Sr_2IrO_4 with nearly 30 to 50% of the Ru^{4+} doping level [32,33]. Interestingly, recent substitution of the $4f$ element in $Sr_2Ir_{1-x}Tb_xO_4$ has shown that a mere 3% of Tb^{4+} completely suppresses the AFM transition while retaining its insulating behavior [34].

In the present work, we have investigated the effect of Cu substitution in $Sr_2Ir_{1-x}Cu_xO_4$, which is rather interesting as Cu^{2+} ($3d^9$) doped for Ir^{4+} ($5d^5$) not only acts for electron doping, but simultaneously tunes both SOC and U, however, in an opposite manner. Another obvious effect would be the change of the Ir charge state from Ir^{4+} to Ir^{5+} ($5d^4$) where later it is believed to be nonmagnetic ($J_{\text{eff}} = 0$) and will act for site dilution. Nonetheless, both Ir^{4+} and Cu^{2+} has single unpaired

*akpramanik@mail.jnu.ac.in

electrons, though they occupy different and orthogonal t_{2g} and e_g orbitals, respectively. It would be very interesting to understand the evolution of the magnetic and electronic behavior in $Sr_2Ir_{1-x}Cu_xO_4$ and to test the compatibility of these orbitals in promoting the magnetism and electronic conduction in this system. Our present work is also motivated to realize the recent calculation which shows an evolution of a PM but spin-orbital ordered Mott phase, particularly doping with elements having extremely weak SOC character which act as a giant perturbation to the spin-orbital structure of Sr_2IrO_4 [35].

Our results show that doped Cu^{2+} substitutes Ir^{4+} and alters the charge state of Ir, producing roughly double the amount of Ir^{5+}. The overall system retains the original structural symmetry, though the lattice parameters and the distortion of IrO_6 octahedra modify with doping of Cu. We observe that with progressive Cu substitution, the long-range magnetic state in Sr_2IrO_4 is destabilized and the system converts to a nearly PM state with ~20% of Cu concentration. The resistivity decreases continuously, but we have not evidenced a metallic state within this studied concentration of Cu. Our analysis shows that temperature-dependent charge conduction is well explained with Mott's two-dimensional (2D) variable-range-hopping (VRH) mechanism.

II. EXPERIMENTAL DETAIL

A series of polycrystalline materials $Sr_2Ir_{1-x}Cu_xO_4$ (x = 0.0, 0.05, 0.10, 0.15, and 0.20) is prepared by the conventional solid-state method. High-purity ingredient components $SrCO_3$, IrO_2, and CuO are mixed in stoichiometric ratio and ground well. The mixed powders are then given several heat treatments in powder and pellet form with intermediate grindings. Finally, samples are prepared after giving heat treatment at 1100 °C. The phase purity of all the materials has been checked by x-ray diffraction (XRD), where the XRD data have been analyzed with the Rietveld refinement program. The XRD data have been collected using a Rigaku diffractometer. Data are collected in the 2θ range 10–90° at an interval of 0.02°. The details of the sample preparation and characterization are reported elsewhere [16,36]. The quantitative analysis of the elemental composition of the present $Sr_2Ir_{1-x}Cu_xO_4$ series has been done with energy-dispersive analysis of x rays (EDX). The obtained molar concentration of ions in $Sr_2Ir_{1-x}Cu_xO_4$ closely matches with the nominal concentration of ions within an error limit of ±3–4%. Further, an x-ray photoemission spectroscopy (XPS) study has been done to probe the oxidation state of iridium and copper. The XPS measurements are performed with base pressure in the range of 10^{-10} mbar using a commercial electron energy analyzer (PHOIBOS 150, Specs GmbH, Germany) and a nonmonochromatic Al$K\alpha$ x-ray source ($h\nu$ = 1486.6 eV). The dc magnetization is measured in a Physical Properties Measurement System (Quantum Design), whereas the electrical transport measurement is done on a homemade system with an Oxford magnet.

III. RESULT AND DISCUSSION

A. Structural characterization

Figure 1(a) shows the XRD pattern of all the samples in the present series. It is evident in the figure that there is no

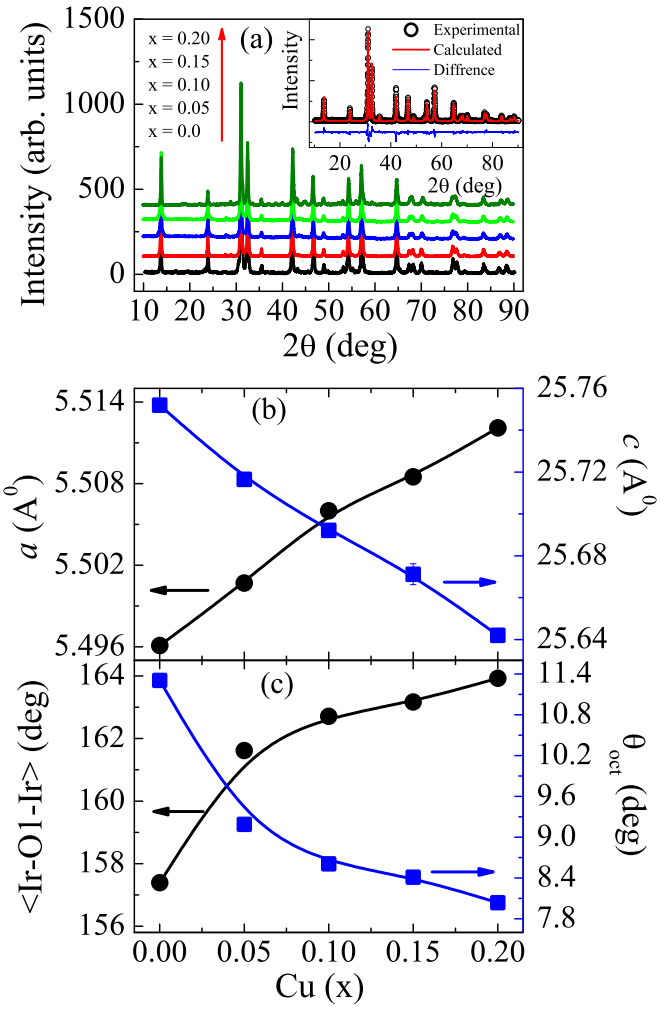

FIG. 1. (a) The XRD pattern for the $Sr_2Ir_{1-x}Cu_xO_4$ series. The inset shows the Rietveld refinement for the x = 0.0 sample. (b) Lattice parameters a (left axis) and c (right axis). (c) Bond angle ⟨Ir-O1-Ir⟩ (left axis) and octahedral rotation θ_{Oct} (right axis) as a function of Cu concentration x. These parameters are determined from Rietveld analysis of powder x-ray diffraction data.

modification in the XRD pattern in terms of peak position or impurity peak with Cu doping, which primarily implies that Cu substitution does not cause any major structural distortion in the present series. The inset of Fig. 1(a) shows representative Rietveld refinement of the XRD data for the x = 0.0 parent material, which suggests reasonably good fitting. The Rietveld analysis shows the sample is in a single phase and crystallizes in a tetragonal structure with $I4_1/acd$ space group. Similarly, Rietveld refinement is performed for other samples in the series with reasonably good fitting. While we find no structural phase transformation with Cu substitution, the lattice parameters show a slight modification with x. Considering a slight mismatch in ionic radii of Ir^{4+} (0.625 Å) and Cu^{2+} (0.73 Å), changes in the lattice parameters are quite expected. Figure 1(b) shows evolution of lattice parameters a and c with Cu concentration. The figure shows a increases and c decreases with x. While these changes in the lattice parameters are not that significant (below 0.4%), the decreasing c/a ratio implies that tetragonal distortion is reduced with progressive

substitution of Cu. Figure 1(c) presents variation of the basal plane Ir-O bond angle (left axis) showing that the ⟨Ir-O1-Ir⟩ angle increases and rather straightens with Cu concentration. The distortion or rotation of the IrO_6 octahedra around the c axis (θ_{oct}) plays a vital role in Sr_2IrO_4, which is believed to induce a Dzyaloshinsky-Moriya (DM)-type antisymmetric exchange interaction and weak ferromagnetic behavior. The right axis of Fig. 1(c) shows variation of θ_{oct} with x. It is evident in the figure that θ_{oct} decreases from 11.3° at $x = 0.0$ to 8.04° at $x = 0.2$. This decrease of θ_{oct} is quite expected as in the Cu-based layered material La_2CuO_4, the CuO_6 octahedra is rotated only by ∼3°, which probably induces stronger AFM behavior and low magnetic moment in this material. Nonetheless, the increase of both lattice parameter a and bond angle ⟨Ir-O1-Ir⟩ and the decrease of θ_{oct} (Fig. 1) are consistent with each other.

B. X-ray photoemission spectroscopy study

It is very important to know the charge state of constituent elements as the ionic state of Cu and the related modification of the Ir charge state will influence the physical properties accordingly. In order to understand the cationic charge distribution in Sr_2IrO_4 as well as its evolution with Cu substitution, we have performed the XPS measurements. Figures 2(a) and 2(b) show the Ir-4f core-level spectra for representative $x = 0.0$ and 0.1, respectively. We have performed a detailed analysis of XPS data using the Voigt function, which includes a convolution of Gaussian and Lorentzian broadenings from different sources. The Ir-4f core-level spectra have been fitted with two peaks corresponding to Ir-4$f_{7/2}$ and Ir-4$f_{5/2}$ levels, observed at the binding energy of 62.0 and 65.0 eV, respectively. The origin of these two peaks is due to spin-orbital splitting with an energy difference of ∼3 eV. The detailed analysis of Ir-4f confirms that the major contribution is coming from the Ir^{4+} states, but there is also a small contribution from the Ir^{5+} ions in the $x = 0.0$ sample; see Fig. 2(a). It is evident in Figs. 2(a) and 2(b) that for Ir^{4+}, the spin-orbit split peaks Ir-4$f_{7/2}$ and Ir-4$f_{5/2}$ arise at binding energy around 62.0 and 65.0 eV, respectively (as shown by the dashed blue lines) [37]. Similarly, Ir-4$f_{7/2}$ and Ir-4$f_{5/2}$ peaks for Ir^{5+} are observed at binding energy 64 and 67.8 eV, respectively (as shown by the dashed green lines). The presence of Ir^{5+} in the parent $x = 0.0$ sample [Fig. 2(a)] is quite interesting. Our analysis reveals that for the Sr_2IrO_4 system, ∼96% of the Ir cations are in the Ir^{4+} ($5d^5$) oxidation state, whereas only ∼4% of Ir are found in the Ir^{5+} ($5d^4$) state. The amount of Ir^{5+} is not substantial though, and possibly arises due to nonstoichiometry of the material. For the doped sample in Fig. 2(b), we observe a significant increase in the Ir^{5+} intensity with respect to the Ir^{4+} states, which qualitatively implies that the Ir^{4+}/Ir^{5+} ratio decreases with Cu substitution. Indeed, our analysis shows that the amount of Ir^{4+} and Ir^{5+} in the $x = 0.1$ sample is about 74 and 26%, respectively. Note that with only 10% of Cu substitution, the amount of Ir^{5+} has increased roughly by 22%, if we consider a similar amount of oxygen nonstoichiometry in the doped material as in the parent material. This result clearly suggests that Cu adopts the charge state of Cu^{2+} and each Cu converts two Ir^{4+} ions into Ir^{5+} ions.

To further comprehend the charge state of Cu in the present series, we have recorded the XPS spectra of Cu $2p_{3/2}$ core level, as presented in Fig. 2(c) for the representative $x = 0.1$ sample. The continuous red line represents the fitting of the XPS data, which is found to be reasonably good. It shows that the Cu-$2p_{3/2}$ spectra is centered around binding energy 933.4 eV, confirming that the Cu is in a Cu^{2+} oxidation state [38]. This result implies that the substitution of each Cu^{2+} converts two Ir^{4+} ions into an Ir^{5+} state. This finding is interesting as following the spin-orbit coupling scheme, Ir^{5+} is believed to be nonmagnetic, which will definitely have a large significance on the magnetic and transport properties in these materials. It is important to note that mostly the physical properties are controlled by the electronic states present near the Fermi level. Therefore, we record XPS valence-band (VB) spectra, as shown in Figs. 2(d) and 2(e) for $x = 0.0$ and 0.1 samples, respectively, and discuss the changes in the states near the Fermi level. For both of the samples, we observed that the Sr-4p peaks at around 20 eV binding energy. We now focus on the near Fermi-level region in which there are no well-defined peaks observed for the $x = 0.0$ sample [see Fig. 2(d)], which is consistent with the higher resistivity and its semiconducting nature. More interesting, with Cu substitution, we observe a relatively sharp peak close to the Fermi level, which is probably due to the contribution mostly from e_g states of the Cu-3d, as marked by a black arrow in Fig. 2(e). This indicates the larger density of states present at the Fermi level for the $x = 0.1$ sample and supports the observed significant decrease in the resistivity at room temperature with Cu substitution. It can be noted here that there is some fluctuation in the XPS-VB data in Fig. 2(d) ($x = 0$), which arises because of the shorter amount of data-collection time given. Nonetheless, both figures show a comparative picture of electronic properties as Fig. 2(e) shows a prominent peak close to the Fermi level in the doped sample which is missing in the parent material.

C. Magnetization study

Figure 3 shows the temperature-dependent magnetization measured under a zero-field-cooled (ZFC) and field-cooled (FC) protocol in an applied field of 10 kOe for the $Sr_2Ir_{1-x}Cu_xO_4$ series. The nature of magnetism in Sr_2IrO_4 is rather interesting. In Sr_2IrO_4, Ir is assumed to adopt the Ir^{4+} charge state, which gives the $5d^5$ electronic state. Due to the high crystal-field effect, all five electrons will populate the low-energy t_{2g} state realizing a low-spin state. In the strong SOC limit, it is believed that the t_{2g} electronic state is split into $J_{eff} = 3/2$ quartet and 1/2 double. In this situation, the $5d^5$ state of Ir^{4+} would give fully filled $J_{eff} = 3/2$ and half-filled $J_{eff} = 1/2$ states. The spin-1/2 of Ir^{4+} otherwise engages in AFM interaction; however, the distortion of the IrO_6 octahedra around the c axis induces a DM-type antisymmetric exchange interaction, which consequently gives weak ferromagnetic behavior with T_c ∼ 225 K [14,36]. Figure 3 depicts $M(T)$ for $x = 0.0$ material and shows a sudden rise below ∼240 K, which marks the PM to (weak) FM transition. On further cooling below ∼95 K, the $M_{ZFC}(T)$ data show a decrease and open a gap between M_{FC} and M_{ZFC}, which has recently been shown to arise due to prominent magnetostructural coupling

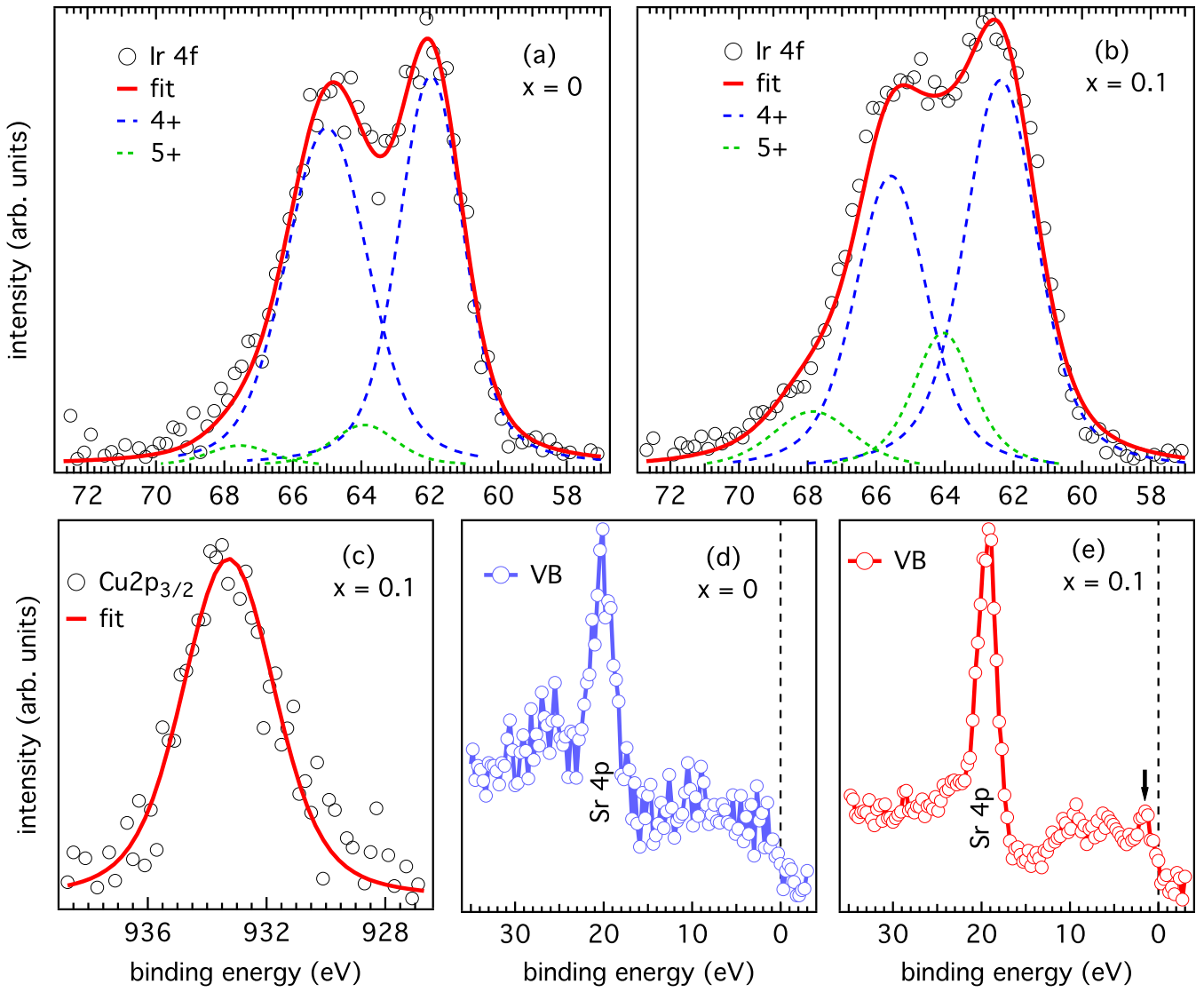

FIG. 2. (a), (b) The Ir $4f$ core-level spectra of $x = 0.0$ and 0.1, respectively. Open black circles represent the experimental data and the red solid lines in (a) and (b) are the fitted envelope taking contributions of Ir^{4+} and Ir^{5+} components, which are individually plotted in dashed blue and green colors, respectively. (c) The Cu $2p_{3/2}$ core-level spectrum of $x = 0.1$ sample. (d), (e) The valence-band spectra with Sr $4p$ states for $x = 0.0$ and 0.1 samples, respectively.

where the spin and lattice degrees of freedom are coupled and suffer staggered rotation with structural evolution with temperature [16]. For the doped materials, along with the decreasing moment, the PM-FM phase transition temperature T_c decreases also with x. This weakening of the FM state is clearly evident for samples with $x = 0.15$ and above where T_c seems to disappear and the $M(T)$ plot looks more like PM samples. This is quite interesting as Cu^{2+} ($3d^9$), which is magnetically active with spin-1/2, substituted for Ir^{4+} ($J_{\text{eff}} = 1/2$) will not act for site dilution, although Cu^{2+} will create a double amount of Ir^{5+} ($J_{\text{eff}} = 0$), which is nonmagnetic and will act for site dilution. However, active d orbitals for the former and latter cations are e_g and t_{2g}, respectively, which are orthogonal so its magnetic compatibility is to be considered. The suppression of long-range magnetic ordering in Sr_2IrO_4 has also been observed when doping with other elements, which is discussed later.

To look into the magnetic state in further detail, we have plotted inverse susceptibility (χ^{-1}) as a function of temperature for this series in Fig. 4(a). For the $x = 0.0$ parent material, $\chi^{-1}(T)$ shows linear behavior above T_c; however, in high temperature above 280 K, the $\chi^{-1}(T)$ deviates from linearity. For doped samples, we also observe similar behavior in the PM state, though $\chi^{-1}(T)$ becomes more linear with x. The Sr_2IrO_4 is known to be a structurally layered material with $n = 1$ in Ruddlesden-Popper series $Sr_{n+1}Ir_nO_{3n+1}$, where the $SrIrO_3$ layer is separated by SrO showing two-dimensional behavior. In fact, a two-dimensional-like anisotropic magnetic interaction for in plane and out of plane has been shown using resonant magnetic x-ray in a diffuse scattering experiment with exchange coupling constant $J \sim 0.1$ and 10^{-6} eV, respectively [14]. This study further shows that in-plane exchange interaction survives at least for ~25 K above $T_N = 228.5$ K. We find that deviation from linearity in our

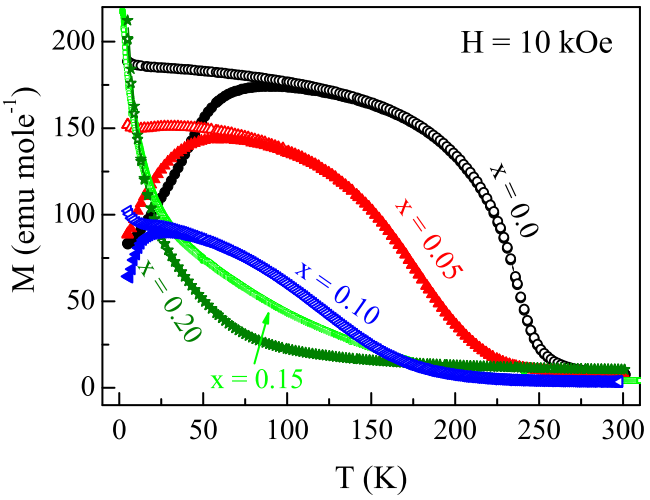

FIG. 3. Magnetizations measured in the applied field of 10 kOe following the ZFC and FC protocol are shown as a function of temperature for the $Sr_2Ir_{1-x}Cu_xO_4$ series.

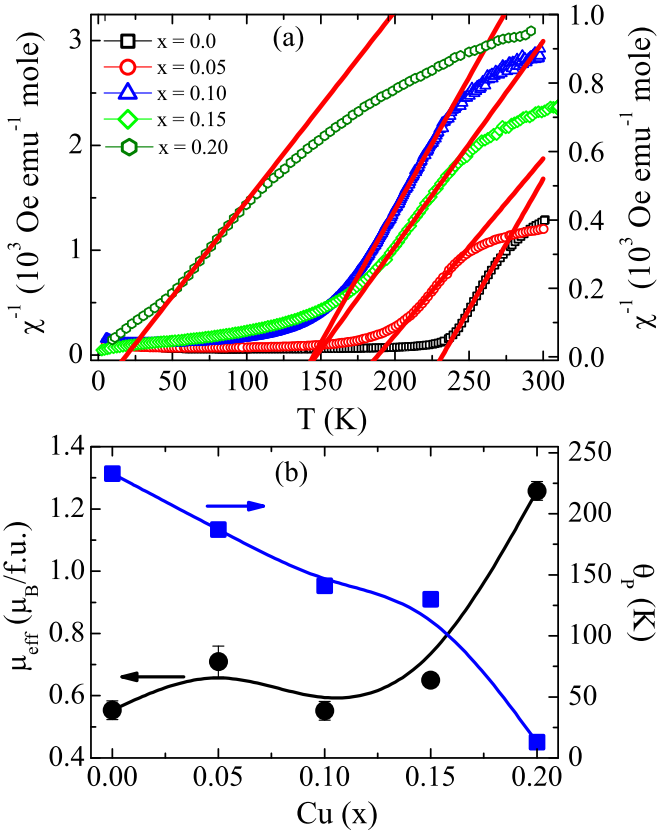

FIG. 4. (a) Temperature-dependent inverse susceptibility [$\chi^{-1} = (M/H)^{-1}$] as deduced from the magnetization data shown in Fig. 3 for a complete series of samples $Sr_2Ir_{1-x}Cu_xO_4$. The solid lines are due to fitting with the Curie-Weiss law [Eq. (1)]. (b) Effective magnetic moment μ_{eff} (left axis) and Curie temperature θ_P (right axis) as a function of Cu, respectively.

$\chi^{-1}(T)$ for Sr_2IrO_4 starts at ~270 K [Fig. 4(a)], which is in qualitative agreement with other microscopic studies. We believe that this change in slope in $\chi^{-1}(T)$ well within the PM state is linked to anisotropic magnetic interaction. However, the persistence of spin correlation at temperatures much higher than the magnetic ordering temperature appears to be a typical feature of layered materials, as seen for La_2CuO_4 [39] or in the case of iron pnictides [40]. In this sense, the increase of linearity of $\chi^{-1}(T)$ with x implies that spin interaction is weakened with Cu doping.

The straight lines in Fig. 4(a) are due to fitting with the Curie-Weiss (CW) law,

$$\chi = \frac{C}{T - \theta_P}, \tag{1}$$

where $C(= N_A\mu_{\text{eff}}^2/3k_B)$ is the Curie constant, μ_{eff} is the effective PM moment, and θ_P is the Curie temperature. Figure 4(a) shows that just above T_c, $\chi^{-1}(T)$ data can be reasonably fitted with Eq. (1). Using the fitted parameter C, we have calculated μ_{eff} for all the samples. Figure 4(b) shows composition-dependent μ_{eff} (left axis) and θ_P (right axis). We calculate $\mu_{\text{eff}} = 0.553\,\mu_B$/f.u. for $x = 0.0$, which appears much lower than the calculated value [for spin-only $g\sqrt{S(S+1)}\mu_B$] of $1.72\,\mu_B$/f.u for spin-1/2 material. The μ_{eff} shows a slight increase in value for $x = 0.05$, which can be due to the active magnetic interaction of Cu in a low-doping regime. With increasing x, although μ_{eff} initially shows some fluctuation, for the highest-doped sample with $x = 0.2$, where $M(T)$ is more like the PM type, it shows a steep increase yielding the value $1.26\,\mu_B$/f.u. While both Ir^{4+} and Cu^{2+} are spin-1/2 elements, Ir^{5+} is believed to be nonmagnetic ($S = 0$). Therefore, for an x amount of Cu^{2+} which generates $2x$ of Ir^{5+}, the average effective moment is $\mu_{\text{eff}} = \sqrt{(1-3x)(^{Ir^{4+}}\mu_{\text{eff}})^2 + 2x(^{Ir^{5+}}\mu_{\text{eff}})^2 + x(^{Cu^{2+}}\mu_{\text{eff}})^2}$, which implies that substitution of Cu would decrease μ_{eff}, provided spins are noninteracting in the PM state. In contrast, a sudden increase of μ_{eff} at a higher value of x suggests that Cu destabilizes the magnetic interaction in Sr_2IrO_4 and promotes the PM state. The composition-dependent θ_P shown in Fig. 4(b) shows that θ_P for parent Sr_2IrO_4 is as high as 233 K, closely matching its $T_c = 225$ K, but the θ_P continuously and sharply decreases with x. Even though θ_P remains positive for the highest $x = 0.2$, its value of 13 K shows that the strength of magnetic interaction is substantially weakened [Fig. 4(b)]. We have not observed any peak or any bifurcation in M_{ZFC} and M_{FC} data in low temperature for $x = 0.2$, but this small and finite value of θ_P probably causes some nonlinearity in $\chi^{-1}(T)$. Nonetheless, Cu^{2+} substituted for Ir^{4+} has a substantial influence on the magnetic behavior of Sr_2IrO_4.

Magnetic-field-dependent magnetization $M(H)$ measured at 5 K in the range of ±70 kOe is shown in Fig. 5(a). The $M(H)$ for Sr_2IrO_4 shows a large opening at low temperatures with coercive field $H_c \sim 9370$ Oe. With Cu substitution, major observations are that the moment μ_H at the highest field increases and H_c substantially decreases, whereas for an $x = 0.2$ material, we find $H_c \sim 100$ Oe. The variations of μ_H and H_c with Cu composition are shown in the upper and lower insets of Fig. 5(a), respectively. In Fig. 5(b), we have shown the Arrott plot of the $M(H)$ data. The Arrott plot (M^2 vs H/M) offers an effective tool to understand the

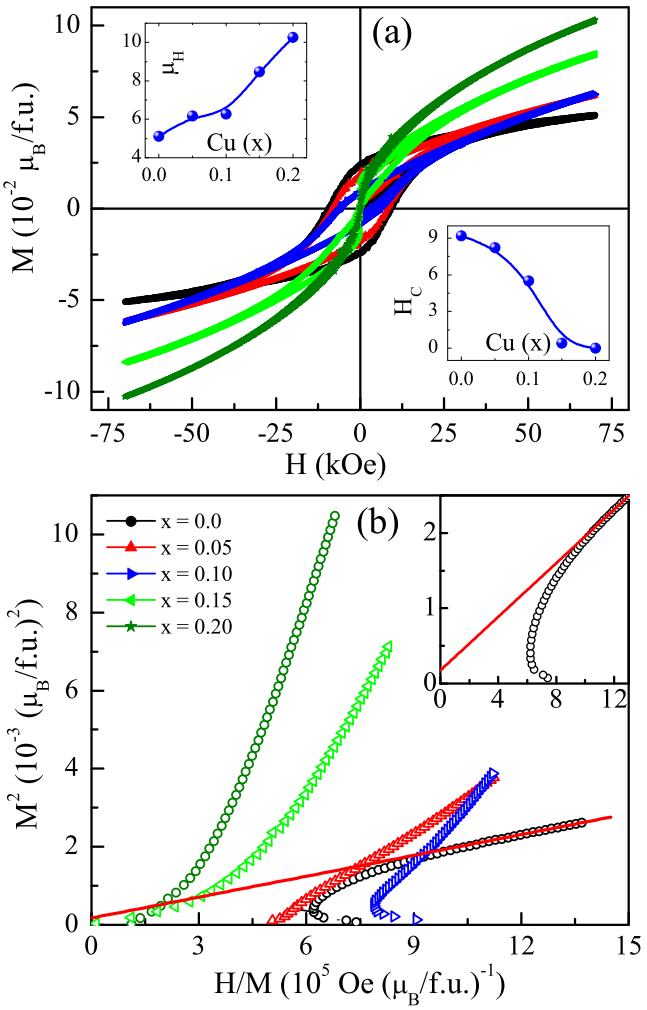

FIG. 5. (a) Isothermal magnetization as a function of the applied field up to ±70 kOe collected at 5 K for the series $Sr_2Ir_{1-x}Cu_xO_4$. The upper and lower insets show the composition-dependent moment μ_H at field 70 kOe and the coercive field H_c, respectively. (b) Arrott plot (M^2 vs H/M) of $M(H)$ data shown in (a). Inset shows magnified view of Arrott plot for the $x = 0.0$ sample close to the origin.

nature of the magnetic state as the positive intercept on the M^2 axis due to a straight-line fitting in high-field regimes of the Arrott plot implies spontaneous magnetization or an FM state. For Sr_2IrO_4, Fig. 5(b) shows a very small positive intercept (magnified view is shown in inset), which indicates weak ferromagnetism in this material, as expected. Cu substitution gives a negative intercept in the Arrott plot, where for higher doping the intercept is highly negative which excludes the possibility of any FM behavior or rather magnetic ordering in the present case. The increase of μ_{eff} and simultaneous decrease of H_c are indicative of weakening of (AFM-type) magnetic ordering, which sets the spins free.

D. Electrical transport

The effect of Cu substitution on charge transport is shown in Fig. 6, which depicts resistivity ρ as a function of temperature for the $Sr_2Ir_{1-x}Cu_xO_4$ series. The Sr_2IrO_4 is a well-known insulator where the intriguing insulating state is believed to

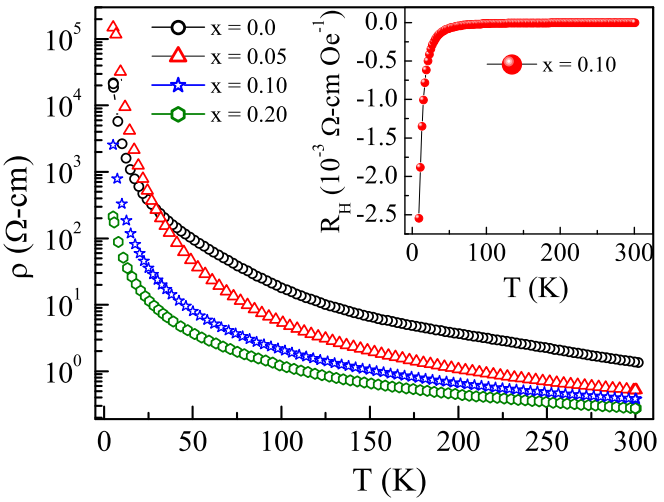

FIG. 6. Temperature-dependent resistivity is shown for the $Sr_2Ir_{1-x}Cu_xO_4$ series. The inset shows the Hall coefficient R_H as a function of temperature in an applied field of 10 kOe.

occur due to opening a gap in the $J_{\text{eff}} = 1/2$ electronic state [10]. Recently, some correlation has been shown between structural, magnetic, and electronic transport behavior in Sr_2IrO_4. The Cu^{2+} is similarly a spin-1/2 system, but its level of d-orbital filling is different compared to Ir^{4+} and acts as electron doping with total $3d^9$ electrons. On the other hand, it will not only tune the SOC and U parameters with its $3d$ character, but it will also create a double amount of Ir^{5+} which has an empty $J_{\text{eff}} = 1/2$ doublet state.

The parent Sr_2IrO_4 shows highly insulating behavior where the resistivity increases by roughly four orders going to low temperatures, in agreement with earlier studies. In doped materials, resistivity decreases continuously with Cu in a higher-temperature regime, but in low temperature, we observe that $\rho(T)$ initially increases for $x = 0.05$ and then decreases. The overall system remains insulating until the highest-doping level ($x = 0.2$). The decrease of resistivity is, however, very prominent in low temperatures. This decrease of resistivity could be caused by many factors, such as the effect of electron doping through Cu^{2+} which would modify the Fermi level, tuning of J_{eff} states through modification of SOC and U, and conversion of Ir^{5+} states which will have empty $J_{\text{eff}} = 1/2$ that would promote hopping of electrons. Hall measurements on Sr_2IrO_4, as reported by Klein *et al.* [41], have shown that charge carriers in this material are hole type, i.e., p-type characteristics of this material. We have tested the temperature dependence of Hall measurements in an applied field of 10 kOe for a selective doped sample, i.e., with $x = 0.1$. The temperature dependence of Hall coefficient $R_H(= 1/ne)$ is shown in the inset of Fig. 6. The negative value of R_H indicates that charge carriers are basically electron type, where this conversion from hole to electron type has occurred through doping of the electron through Cu^{2+} substitution.

In an attempt to understand the nature of charge conduction in the present series, we found that resistivity can be best explained using a thermally activated conduction mechanism

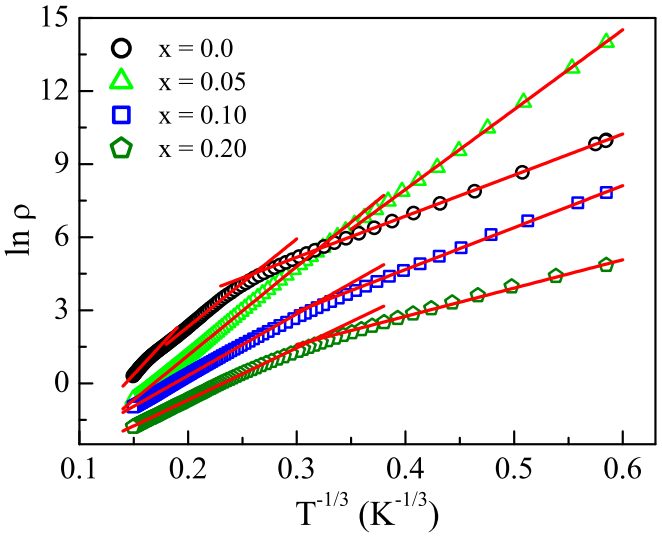

FIG. 7. Logarithm of resistivity with $T^{-1/3}$ is shown for $Sr_2Ir_{1-x}Cu_xO_4$. The solid lines are the least-squares fitting due to the two-dimensional Mott variable-range-hopping model following Eq. (2) in different temperature ranges. The data for $x = 0.20$ have been shifted downward for clarity.

described by a two-dimensional (2D) Mott variable-range-hopping (VRH) model [42],

$$\rho = \rho_0 \exp\left[\left(\frac{T_0}{T}\right)^{1/3}\right], \tag{2}$$

where T_0 is the characteristic temperature and can be expressed as

$$T_0 = \frac{21.2}{k_B N(E_F)\xi^3}, \tag{3}$$

where k_B is the Boltzmann constant, $N(E_F)$ is the density of states (DOS) at the Fermi level, and ξ is the localization length.

Here it should be noted that we have previously shown that charge conduction in Sr_2IrO_4 follows the Mott 2D variable-range-hopping model in three different temperature regimes, which are related to the magnetic and/or structural state in this material [16]. Moreover, the 2D nature of charge transport is in agreement with the layered structure of Sr_2IrO_4. Taking this as a guideline, we have analyzed the $\rho(T)$ data for all of the compositions using Eq. (2). Figure 7 shows a straight-line fitting of the $\rho(T)$ data following Eq. (2), where for parent Sr_2IrO_4, the data can be fitted in three distinct temperature regimes. The temperature regimes and obtained fitting parameters T_0 are given in Table I. The temperature regimes mark the change of magnetic state (Fig. 3) and structural parameters [16]. For the doped samples, however, we can fit the data only in two distinct temperature regimes (Fig. 7). The temperatures ranges and the parameter T_0 are given in Table I. This could be understood as magnetic transitions in doped materials are broadened which has led to single temperature fitting behavior in high temperatures. Nonetheless, the change of slope in Fig. 7 for the $x = 0.2$ compound is intriguing as magnetization data show no clear magnetic transition. This could be due to the existence of a short-range type of magnetic ordering as evident in $\chi^{-1}(T)$ where a slope change is observed at low temperatures [Fig. 4(a)].

TABLE I. Temperature range and fitting parameter T_0 obtained from the fitting of Eq. (2) in Fig. 7 are given for the $Sr_2Ir_{1-x}Cu_xO_4$ series.

Sample $Sr_2Ir_{1-x}Cu_xO_4$	Temperature range (K)	T_0 (K) (10^5)
$x = 0.0$	300–240	1.44(1)
	240–70	0.46(8)
	40–5	0.04(8)
$x = 0.05$	300–35	0.48(6)
	30–5	0.35(2)
$x = 0.10$	300–33	0.16(1)
	25–5	0.05(1)
$x = 0.20$	300–30	0.11(4)
	20–5	0.02(1)

Table I further indicates that parameter T_0 shows a lower value both with lowering the temperature as well as with increasing the Cu concentration. For Sr_2IrO_4, we have previously shown that the change of T_0 with lowering of temperature can be explained through an increase of localization length ξ as $N(E_F)$ would unlikely modify for an insulating sample [Eq. (3)] [16]. However, the modification of T_0 with x cannot be straightforwardly explained as an increase of both $N(E_F)$ and the ξ parameter can contribute to a decrease of T_0. This is a quite likely phenomenon as modification of the electronic conductivity (Fig. 6), structural parameters (Fig. 1), and magnetic state (Fig. 3) with Cu indicates that both $N(E_F)$ and ξ would possibly change with x. Nonetheless, a large change in conductivity in the $Sr_2Ir_{1-x}Cu_xO_4$ series implies that $N(E_F)$ has major contributions for change of T_0.

For further understanding of electronic transport behavior, we have measured the electrical resistivity in the presence of magnetic field at 5 K. Figure 8 shows the change of resistivity, which is commonly known as magnetoresistance

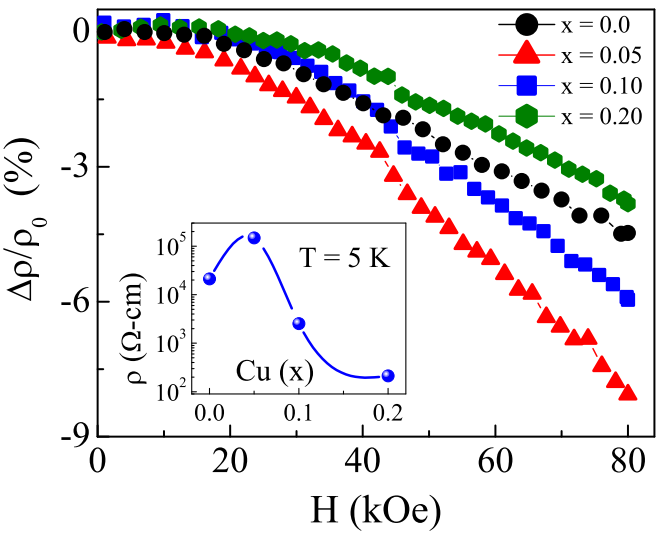

FIG. 8. Magnetoresistance measured at 5 K in magnetic field up to 80 kOe is shown for the $Sr_2Ir_{1-x}Cu_xO_4$ series. The inset shows the variation of resistivity with doping concentration x at 5 K.

(MR) and calculated as $\Delta\rho/\rho(0) = [\rho(H) - \rho(0)]/\rho(0)$ for the $Sr_2Ir_{1-x}Cu_xO_4$ series. All of the samples show negative MR, i.e., conductivity increases in the presence of a magnetic field. In the picture of variable range hopping, negative MR is considered to arise due to the "weak-localization" phenomenon, induced by the quantum interference effect [43,44]. Recently, we have shown that parent Sr_2IrO_4 exhibits negative MR and its quadratic field dependence which is considered as a typical feature of the weak-localization effect [16]. Figure 8 shows that the evolution of MR with field is not linear where the resistivity starts to decrease above ~20 kOe. The MR value is not, however, substantial and Sr_2IrO_4 shows ~4.5% MR in the field as high as 80 kOe. As Cu is introduced, the general feature of MR with field remains similar, but its magnitude initially increases, showing the highest value for $x = 0.05$, and then decreases. While the exact reason for this anomalous change of MR is not very clear, in a lower concentration of Cu, i.e., for $x = 0.05$, we have already seen some anomaly in the magnetic moment, μ_{eff} and μ_H, in Figs. 4(b) and 5(a), respectively. Moreover, it is evident in Fig. 6 that resistivity at low temperatures initially increases with x. In the inset of Fig. 8, we have shown composition-dependent resistivity value at 5 K in the zero field, showing a nonmonotonic behavior. While the structural parameters do not exhibit any anomalous behavior for low-doped samples (Fig. 1), this anomaly in the magnetic moment as well as in electronic transport behavior for $x = 0.05$ samples appears to be a correlated effect. From these observations, we speculate that Cu in a lower concentration induces the magnetic moment, which perhaps inhibits the hopping of charge carriers (VRH), and hence resistivity increases at low temperatures. The application of a magnetic field tends to orient the moments which may be helpful for the hopping mechanism, and therefore negative MR increases. In a higher concentration of Cu, along with an increase of electrons, the Ir^{5+} also increases which can reverse the situation.

E. Possible ionic arrangement and interaction model

Our studies show that Cu substitution in the $Sr_2Ir_{1-x}Cu_xO_4$ series has prominent effects on the magnetism and electronic transport behavior where the magnetic state is largely weakened, giving PM-like behavior for an $x = 0.2$ material, and the charge conductivity overall increases. The similar weakening or suppression of magnetic ordering and the insulating state has previously been observed in Sr_2IrO_4 with different chemical substitution. For Sr-site doping with La^{3+}, which acts for electron doping creating an equivalent amount of Ir^{3+} ($5d^6$), the magnetic state is completely suppressed with ~3% of doping concentration in $(Sr_{1-x}La_x)_2IrO_4$ [28,29]. In the case of Ir-site doping, results with different elements are different. For instance, Tb^{4+} substitution, which is believed to change the relative strength of SOC, crystal-field effect, and Hund's coupling with its $4f^7$ character cause complete suppression of the magnetic state with a mere 3% of doping concentration [34]. While the charge state of Rh is debated (Rh^{3+} or Rh^{4+} which would induce hole or isoelectronic doping, respectively), its substitution in $Sr_2Ir_{1-x}Rh_xO_4$ has shown suppression of the ordered magnetic and insulating state above the critical doping concentration of ~17% [30,31,45]. Similarly, Ru substitution has caused suppression of magnetic ordering in Sr_2IrO_4 with nearly 30 to 50% of Ru^{4+} doping level [32,33].

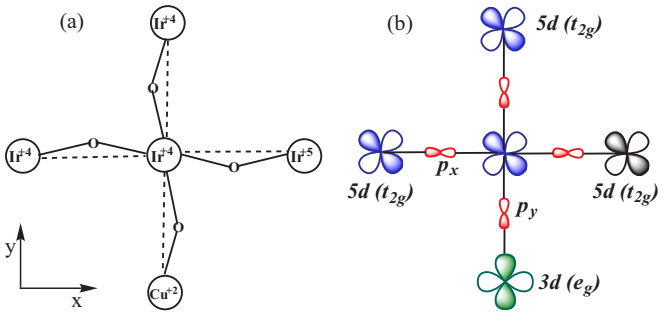

FIG. 9. (a) Visualization of possible arrangement of Ir^{4+}, Ir^{5+}, and Cu^{2+} ions. (b) The schematic arrangement of Cu-3d and Ir-5d orbitals is shown.

In the present $Sr_2Ir_{1-x}Cu_xO_4$ series, both Ir^{4+} and Cu^{2+} are spin-1/2 element and magnetically active; however, their respective orbitals are not symmetric. For instance, in a strong SOC limit, Ir^{4+} has a half-filled $J_{\text{eff}} = 1/2$ state (t_{2g}) while the single spin in Cu^{2+} populates the $d_{x^2-y^2}$ orbital (e_g). The incompatibility of magnetic interaction between transition metals with orthogonal d character has been discussed for spin chain material Sr_3MIrO_6 (M = Ni, Co) [46]. In addition, Cu^{2+} substitution will create a double amount of Ir^{5+} ($5d^4$), which are expected to be nonmagnetic considering four electrons will fully fill the $J_{\text{eff}} = 3/2$ quartet state. In transition-metal oxides, the metal octahedra are generally corner shared and the magnetic interactions are mediated through O-2p orbitals. While ionic distribution is quite random, based on the present scenario, the magnetic interaction scheme is depicted in Fig. 9. Since the Ir^{5+} is nonmagnetic, exchange interaction through the Ir^{4+}-O^{2-}-Ir^{5+} channel is very unlikely; however, the same through the Ir^{4+}-O^{2-}-Ir^{4+} and Ir^{4+}-O^{2-}-Cu^{2+} channels is of interest. Note that in trivalent-doped $(Sr_{1-x}La_x)_2IrO_4$, where La^{3+} doping creates Ir^{3+} ($5d^6$) ions which are again nonmagnetic (fully filled $J_{\text{eff}} = 3/2$ quartet and $J_{\text{eff}} = 1/2$ doublet states), the long-range magnetic ordering is suppressed with only ~3% of La doping [28]. In contrast, magnetism survives until a higher-doping level (~20%) of Cu^{2+} substitution at the Ir site in the present study. Similar results are also evident for Rh^{3+} and Ru^{4+} where magnetism is totally suppressed with ~17 and 30% of doping concentration, respectively [30,32]. Given that Rh^{3+} and Cu^{2+} create nonmagnetic Ir^{5+}, both have similarity as they create a double amount of nonmagnetic sites: Rh^{3+} and Ir^{5+} in the former case and Ir^{5+} and Ir^{5+} in the latter case. Of course, since Cu^{2+} is magnetic, effective magnetic exchange would be different and complex compared to Rh^{3+}. For 20% of Cu, magnetic interaction is substantially weakened and is almost suppressed, though we find some trace of magnetism. Thus, like Rh^{3+} doping [30], the percolation picture to explain the suppression of magnetism apparently looks valid for Cu^{2+} also. The evolution of magnetic and transport properties with x in $Sr_2Ir_{1-x}Cu_xO_4$ is quite intriguing and needs to be investigated using microscopic probe as well as theoretical models.

IV. CONCLUSION

In conclusion, we have studied the structural, magnetic, and electronic transport properties in a series of polycrystalline samples $Sr_2Ir_{1-x}Cu_xO_4$ with $x \leqslant 0.2$. Structural investigation shows that while the system retains its original structural symmetry, the unit-cell parameters modify with Cu. In particular, both the c/a ratio and distortion of IrO_6/CuO_6 octahedra decrease with x. The XPS results reveal that doped Cu^{2+} converts a double amount of Ir^{4+} into Ir^{5+} and sharpens the valence-band spectra at the Fermi level. Substitution of Cu^{2+} introduces electron doping, which is evident in Hall measurements. Long-range magnetic ordering in parent material Sr_2IrO_4 is destabilized with Cu and in the highest-doped sample, i.e., in $Sr_2Ir_{0.8}Cu_{0.2}O_4$, the magnetic data show paramagneticlike behavior. However, resistivity decreases but the system does not become metallic with the available 20% of Cu doping. The charge conduction follows the Mott 2D VRH model, but interestingly the validity of this model changes with temperature and appears to follow the magnetic behavior. A weak negative MR has been observed at low temperature, which is considered to be a signature of a weak-localization effect in a spin-orbit coupled system. The evolution of MR shows nonmonotonic behavior with Cu substitution; its appears to instead follow the variation of resistivity with x.

ACKNOWLEDGMENTS

We acknowledge UGC-DAE CSR, Indore and Alok Banerjee, Rajeev Rawat, and Archana Lakhani for magnetization, resistivity, and Hall measurements. We also thank Kranti Kumar and Sachin Kumar for assistance with the measurements. I.N.B. acknowledges the financial support of CSIR, India through a fellowship.

[1] J. G. Rau, E. K.-H. Lee, and H.-Y. Kee, Annu. Rev. Condens. Matter Phys. **7**, 195 (2016).
[2] W. Witczak-Krempa, G. Chen, Y. B. Kim, and L. Balents, Annu. Rev. Condens. Matter Phys. **5**, 57 (2014).
[3] G. Cao and P. Schlottmann, arXiv:1704.06007.
[4] G. Cao, A. Subedi, S. Calder, J.-Q. Yan, J. Yi, Z. Gai, L. Poudel, D. J. Singh, M. D. Lumsden, A. D. Christianson, B. C. Sales, and D. Mandrus, Phys. Rev. B **87**, 155136 (2013).
[5] S. Calder, G.-X. Cao, S. Okamoto, J. W. Kim, V. R. Cooper, Z. Gai, B. C. Sales, M. D. Lumsden, D. Mandrus, and A. D. Christianson, Phys. Rev. B **89**, 081104 (2014).
[6] X. Wan, A. M. Turner, A. Vishwanath, and S. Y. Savrasov, Phys. Rev. B **83**, 205101 (2011).
[7] W.-G. Yin, X. Liu, A. M. Tsvelik, M. P. M. Dean, M. H. Upton, J. Kim, D. Casa, A. Said, T. Gog, T. F. Qi, G. Cao, and J. P. Hill, Phys. Rev. Lett. **111**, 057202 (2013).
[8] R. Dally, T. Hogan, A. Amato, H. Luetkens, C. Baines, J. Rodriguez-Rivera, M. J. Graf, and S. D. Wilson, Phys. Rev. Lett. **113**, 247601 (2014).
[9] H. Kumar and A. K. Pramanik, J. Magn. Magn. Mater. **409**, 20 (2016).
[10] B. J. Kim, Hosub Jin, S. J. Moon, J.-Y. Kim, B.-G. Park, C. S. Leem, Jaejun Yu, T. W. Noh, C. Kim, S.-J. Oh, J.-H. Park, V. Durairaj, G. Cao, and E. Rotenberg, Phys. Rev. Lett. **101**, 076402 (2008).
[11] B. J. Kim, H. Ohsumi, T. Komesu, S. Sakai, T. Morita, H. Takagi, and T. Arima, Science **323**, 1329 (2009).
[12] M. K. Crawford, M. A. Subramanian, R. L. Harlow, J. A. Fernandez-Baca, Z. R. Wang, and D. C. Johnston, Phys. Rev. B **49**, 9198 (1994).
[13] F. Ye, S. Chi, B. C. Chakoumakos, J. A. Fernandez-Baca, T. Qi, and G. Cao, Phys. Rev. B **87**, 140406 (2013).
[14] S. Fujiyama, H. Ohsumi, T. Komesu, J. Matsuno, B. J. Kim, M. Takata, T. Arima, and H. Takagi, Phys. Rev. Lett. **108**, 247212 (2012).
[15] G. Jackeli and G. Khaliullin, Phys. Rev. Lett. **102**, 017205 (2009).
[16] I. N. Bhatti, R. Rawat, A. Banerjee, and A. K. Pramanik, J. Phys.: Condens. Matter **27**, 016005 (2014).
[17] J. M. Tarascon, L. H. Green, W. R. McKinnon, G. W. Hull, and T. H. Geballe, Science **235**, 1373 (1987).
[18] E. S. Bozin, S. J. L. Billinge, G. H. Kwei, and H. Takagi, Phys. Rev. B **59**, 4445 (1999).
[19] Y. Maeno, H. Hashimoto, K. Yoshida, S. Nishizaki, T. Fujita, J. G. Bednorz, and F. Lichtenberg, Nature (London) **372**, 532 (1994).
[20] A. P. Mackenzie, R. K. W. Haselwimmer, A. W. Tyler, G. G. Lonzarich, Y. Mori, S. Nishizaki, and Y. Maeno, Phys. Rev. Lett. **80**, 3890 (1998).
[21] Y. Yang, W.-S. Wang, J.-G. Liu, H. Chen, J.-H. Dai, and Q.-H. Wang, Phys. Rev. B **89**, 094518 (2014).
[22] Y. Gao, T. Zhou, H. Huang, and Q.-H. Wang, Sci. Rep. **5**, 9251 (2015).
[23] J. Kim, D. Casa, M. H. Upton, T. Gog, Y.-J. Kim, J. F. Mitchell, M. van Veenendaal, M. Daghofer, J. van den Brink, G. Khaliullin, and B. J. Kim, Phys. Rev. Lett. **108**, 177003 (2012).
[24] Y. J. Yan, M. Q. Ren, H. C. Xu, B. P. Xie, R. Tao, H. Y. Choi, N. Lee, Y. J. Choi, T. Zhang, and D. L. Feng, Phys. Rev. X **5**, 041018 (2015).
[25] S. Sumita, T. Nomoto, and Y. Yanase, Phys. Rev. Lett. **119**, 027001 (2017).
[26] Y. K. Kim, O. Krupin, J. D. Denlinger, A. Bostwick, E. Rotenberg, Q. Zhao, J. F. Mitchell, J. W. Allen, and B. J. Kim, Science **345**, 187 (2014).
[27] A. de la Torre, S. McKeown Walker, F. Y. Bruno, S. Riccó, Z. Wang, I. Gutierrez Lezama, G. Scheerer, G. Giriat, D. Jaccard, C. Berthod, T. K. Kim, M. Hoesch, E. C. Hunter, R. S. Perry, A. Tamai, and F. Baumberger, Phys. Rev. Lett. **115**, 176402 (2015).
[28] X. Chen, T. Hogan, D. Walkup, W. Zhou, M. Pokharel, M. Yao, Wei Tian, T. Z. Ward, Y. Zhao, D. Parshall, C. Opeil, J. W. Lynn, V. Madhavan, and S. D. Wilson, Phys. Rev. B **92**, 075125 (2015).
[29] H. Gretarsson, N. H. Sung, J. Porras, J. Bertinshaw, C. Dietl, Jan A. N. Bruin, A. F. Bangura, Y. K. Kim, R. Dinnebier, J. Kim, A. Al-Zein, M. Moretti Sala, M. Krisch, M. Le Tacon, B. Keimer, and B. J. Kim, Phys. Rev. Lett. **117**, 107001 (2016).
[30] J. P. Clancy, A. Lupascu, H. Gretarsson, Z. Islam, Y. F. Hu, D. Casa, C. S. Nelson, S. C. LaMarra, G. Cao, and Y.-J. Kim, Phys. Rev. B. **89**, 054409 (2014).

[31] T. F. Qi, O. B. Korneta, L. Li, K. Butrouna, V. S. Cao, X. Wan, P. Schlottmann, R. K. Kaul, and G. Cao, Phys. Rev. B **86**, 125105 (2012).

[32] S. Calder, J. W. Kim, G.-X. Cao, C. Cantoni, A. F. May, H. B. Cao, A. A. Aczel, M. Matsuda, Y. Choi, D. Haskel, B. C. Sales, D. Mandrus, M. D. Lumsden, and A. D. Christianson, Phys. Rev. B **92**, 165128 (2015).

[33] S. J. Yuan, S. Aswartham, J. Terzic, H. Zheng, H. D. Zhao, P. Schlottmann, and G. Cao, Phys. Rev. B **92**, 245103 (2015).

[34] J. C. Wang, S. Aswartham, F. Ye, J. Terzic, H. Zheng, D. Haskel, S. Chikara, Y. Choi, P. Schlottmann, R. Custelcean, S. J. Yuan, and G. Cao, Phys. Rev. B. **92**, 214411 (2015).

[35] C. Martins, M. Aichhorn, L. Vaugier, and S. Biermann, Phys. Rev. Lett. **107**, 266404 (2011).

[36] I. N. Bhatti and A. K. Pramanik, J. Magn. Magn. Mater. **422**, 141 (2017).

[37] W. K. Zhu, M. Wang, B. Seradjeh, F. Yang, and S. X. Zhang, Phys. Rev. B **90**, 054419 (2014).

[38] M. S. Kim, J. B. Yang, J. Medvedeva, W. B. Yelon, P. E. Parris, and W. J. James, J. Phys.: Condens. Matter **20**, 255228 (2008).

[39] B. Keimer, N. Belk, R. J. Birgeneau, A. Cassanho, C. Y. Chen, M. Greven, M. A. Kastner, A. Aharony, Y. Endoh, R. W. Erwin, and G. Shirane, Phys. Rev. B **46**, 14034 (1992).

[40] R. Klingeler, N. Leps, I. Hellmann, A. Popa, U. Stockert, C. Hess, V. Kataev, H.-J. Grafe, F. Hammerath, G. Lang, S. Wurmehl, G. Behr, L. Harnagea, S. Singh, and B. Büchner, Phys. Rev. B **81**, 024506 (2010).

[41] Y. Klein and I. Terasaki, J. Electron. Mater. **38**, 1331 (2009).

[42] N. Mott, *Conduction in Non-Crystalline Materials* (Clarendon, Oxford, 1993).

[43] V. L. Nguyen, B. Z. Spivak, and B. I. Shklovskii, Zh. Eksp. Teor. Fiz. **89**, 1770 (1985) [Sov. Phys. JETP **62**, 1021 (1985)].

[44] U. Sivan, O. Entin-Wohlman, and Y. Imry, Phys. Rev. Lett. **60**, 1566 (1988).

[45] Y. Cao, Q. Wang, J. A. Waugh, T. J. Reber, H. Li, X. Zhou, S. Parham, S.-R. Park, N. C. Plumb, E. Rotenberg, A. Bostwick, J. D. Denlinger, T. Qi, M. A. Hermele, G. Cao, and D. S. Dessau, Nat. Commun. **7**, 11367 (2016).

[46] X. Ou and H. Wu, Sci. Rep. **4**, 04609 (2014).